Interplanetary Cruising

1. Foreword

The following material is intended to supplement NASA-JSC's High School Aerospace Scholars (HAS) instructional reading. The author, a retired veteran of 60 Space Shuttle flights at Mission Control's Flight Dynamics Officer (FDO) Console, first served as HAS mentor in association with a June 2008 workshop. On that occasion, he noticed students were generally unfamiliar with the nature and design of spacecraft trajectories facilitating travel between Earth and Mars. Much of the specific trajectory design data appearing herein was developed during that and subsequent workshops as reference material for students integrating it into Mars mission timeline, spacecraft mass, landing site selection, and cost estimates. *Interplanetary Cruising* is therefore submitted to HAS for student use both before and during Mars or other interplanetary mission planning workshops.

Notation in this document distinguishes vectors from scalars using **bold** characters in a vector's variable name. The "•" operator denotes a scalar product between two vectors. If vectors $\boldsymbol{a}$ and $\boldsymbol{b}$ are represented with scalar coordinates such that $\boldsymbol{a} = (a_1, a_2, a_3)$ and $\boldsymbol{b} = (b_1, b_2, b_3)$ in some 3-dimensional Cartesian system, $\boldsymbol{a} \bullet \boldsymbol{b} = a_1 b_1 + a_2 b_2 + a_3 b_3 = a\, b \cos \gamma$, where γ is the angle between $\boldsymbol{a}$ and $\boldsymbol{b}$.

2. Introduction

Material in this reference will help us understand the pedigree and limitations applying to paths (trajectories) followed by spacecraft about the Sun as they "cruise" through interplanetary space. Although cruise between Earth and Mars is used in specific examples, this lesson's physics would apply to travel between any two reasonably isolated objects in our solar system. The most advanced propulsion systems in existence now permit interplanetary travel under continuous thrust, but we'll simplify these more exotic trajectories by assuming all our spacecraft's rocket power is delivered as we depart or arrive at Earth or Mars. In effect, our cruise will be a coast subject only to acceleration from gravity.

As modeled by Johannes Kepler in 1605 to high accuracy, the orbits of Earth and Mars about the Sun are ellipses with the Sun lying at one focus. This principle is known as Kepler's First Law and is a manifestation of Isaac Newton's Law of Universal Gravitation published in 1687. Except for a few days after departing or before arriving at Earth or Mars, our coasting spacecraft's trajectory is only affected to an appreciable extent by solar gravitational acceleration and obeys Kepler's First Law too. Consequently, we'll make the further assumption that interplanetary cruise is only subject to acceleration from the Sun's gravity.

The Sun-centered (heliocentric) elliptical motion assumption lets us invoke a very powerful spacecraft trajectory design technique known as Lambert's Theorem. Published by Johann Lambert in 1761, Lambert's Theorem relates cruise time Δt between Earth and Mars to three geometric quantities. Each of the geometric quantities, defined below, is illustrated in Figure 1 for an example spacecraft trajectory from Earth to Mars.

Interplanetary Cruising

$a \equiv$ mean solar distance (semi-major axis) pertaining to the interplanetary cruise ellipse

$r_D + r_A \equiv$ the sum of heliocentric distances at departure and arrival in the interplanetary cruise ellipse

$c \equiv$ the distance (chord) between heliocentric departure and arrival positions in the interplanetary cruise ellipse

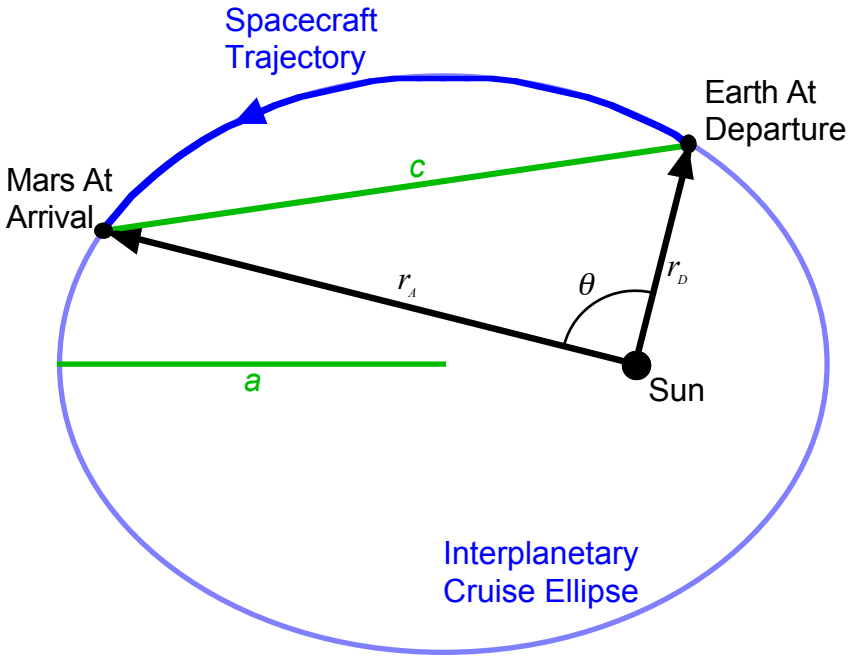

Figure 1. Lambert's Theorem parameters are illustrated in a heliocentric Earth-to-Mars interplanetary cruise ellipse. The difference between r_D and r_A is exaggerated for clarity. Roughly spherical regions of space in which Earth and Mars gravity dominate the Sun's have radii less than 1% of r_D. Consequently, the heliocentric cruise ellipse accurately describes 99% of the Earth-to-Mars trajectory. The heliocentric transfer angle θ is also illustrated.

We'll use the "patched conic" approximation to seamlessly merge a heliocentric interplanetary cruise ellipse with a planet-centered hyperbolic trajectory near departure or arrival. Because a planet's gravity field is miniscule on the scale of the Sun's, velocity in the Sun-centered ellipse becomes *asymptotic* velocity in the planet-centered hyperbola when the planet's heliocentric velocity is subtracted from our spacecraft's heliocentric velocity. Magnitude of the planet-centered asymptotic velocity is termed s_D at departure, s_A at arrival, and hyperbolic excess speed v_{HE} generically. The "excess" speed is with respect to a marginal parabolic escape into interplanetary space with zero v_{HE}. In other references, v_{HE} is termed v_∞ because this velocity is asymptotically approached in the limit of infinite planet-centered distance.

To planet-centered trajectories, we'll apply the principle of total energy (kinetic plus potential) invariance, known as the *vis viva* energy integral. With the energy integral, we can compute planet-centered velocity magnitude (speed) at any planet-centered distance along a specific conic trajectory if we know speed at any other distance along that same trajectory. We're then able to

compute the change-in-velocity magnitude Δv associated with injecting our spacecraft into one trajectory from another.

Finally, we'll use the *rocket equation* to relate a specified Δv, our spacecraft's mass, payload mass aboard our spacecraft, and propulsive efficiency to the propellant mass required to achieve Δv. The rocket equation is typically applied in *stages* such that total mass before Δv is imparted, or some logical component of it, is equivalent to payload mass in the previous stage. In this manner, total mass prior to Earth departure can be estimated and related to mission cost. This cost-driving relationship is informally referred to as "the tyranny of the rocket equation" in the field of astronautics.

3. Lambert Solutions

Lambert's Theorem is typically applied to solution of a boundary value problem in which departure time t_D and departure planet are specified, together with arrival time t_A and arrival planet. These Lambert boundary conditions (LBCs) are used with well-documented theories of Earth and Mars orbit motion (ephemerides) to generate heliocentric vector positions $\boldsymbol{r}_D$ and $\boldsymbol{r}_A$. From these positions, scalars r_D, r_A, and c are readily computed, and $\Delta t = t_A - t_D$. The Lambert equation relating Δt to a, $r_D + r_A$, and c is then iteratively solved for a, defining the interplanetary cruise ellipse.

The spacecraft trajectory illustrated by Figure 1 is known as a "short-way" Lambert solution because its heliocentric arc subtends a transfer angle $\theta < 180°$. A second Lambert solution defined by Figure 1's $\boldsymbol{r}_D$ and $\boldsymbol{r}_A$ is the "long-way" trajectory on a different interplanetary cruise ellipse[1] and subtending $360° - \theta > 180°$. In practice, we'll therefore supplement LBCs with a short-way/long-way choice. For otherwise identical LBCs, we'll find it easy to exclude either the short-way or long-way solution from further consideration because one of these two trajectories will cruise about the Sun in a direction contrary (retrograde) to that of Earth and Mars. Getting our spacecraft onto a retrograde heliocentric trajectory is Δv-prohibitive because the departure planet's speed about the Sun must first be cancelled before additional motion in the opposite direction is imparted. To minimize propellant consumption, our spacecraft trajectory must match departure planet heliocentric velocity at departure (and arrival planet heliocentric velocity at arrival) as closely as possible.

There's actually a further proliferation of Lambert solutions defined by $\boldsymbol{r}_D$ and $\boldsymbol{r}_A$ if we're willing to increase Δt to more than an orbit period in the interplanetary cruise ellipse. We'll ignore solutions with $\theta \geq 360°$ in this discussion, as we're not interested in cruising to and from Mars any longer than necessary.

Finally, we should be acutely aware of Lambert solutions with θ near 180° that are marginally short-way or long-way. Corresponding spacecraft trajectories are very nearly Hohmann transfers, sometimes cited as the most propellant-efficient interplanetary trajectories. This would

[1] If Δt is too small, the long-way solution may require speed sufficient to escape the solar system. Under these conditions, the interplanetary trajectory becomes a hyperbola.

indeed be the case if departure and arrival heliocentric planetary orbits were exactly co-planar. Unfortunately, Mars's orbit plane is tilted (inclined) 1.85° with respect to Earth's (the ecliptic). When $\boldsymbol{r}_D$ and $\boldsymbol{r}_A$ are very nearly in opposite directions from the Sun, our spacecraft's trajectory plane is poorly defined. Consequently, Mars's ecliptic inclination can produce Lambert solutions with ecliptic inclinations approaching 90° when θ is near 180°.

Near-Hohmann cruise trajectories are usually extreme "gas-guzzlers" because departing the ecliptic plane always entails a large spacecraft velocity change at Earth and Mars. The only exception would be the very special case when θ is exactly 180° and Mars lies at one of two points (nodes) where its orbit crosses the ecliptic exactly as your spacecraft arrives at or departs from Mars. In these unlikely cases, Lambert solutions may still have appreciable ecliptic inclinations depending on how co-linear $\boldsymbol{r}_D$ and $\boldsymbol{r}_A$ are interpreted by solution computations. Geometrically speaking, $\theta = 180°$ is a Lambert Theorem singularity leading to an infinite number of equally valid solutions corresponding to all possible heliocentric planes.

With these Lambert Theorem fundamentals understood, we're equipped to design coasted interplanetary cruise trajectories using "minimum impulse" while we await invention of the warp drive. In the following section, we'll learn how to organize and interpret large numbers of Lambert solutions in order to optimize interplanetary trajectories for minimal propellant consumption.

4. The *Pork Chop* Chart (PCC)

A PCC is a two-dimensional matrix of values from an ordered array of Lambert solutions. The element value assigned to each solution in the matrix "maps" a third dimension and may be any single variable relatable to all the solutions. In PCC examples to follow, we will confine ourselves to planet-centered departure speed s_D or arrival speed s_A matrix values[2]. Each column in the matrix pertains to a particular Lambert solution departure time t_D, and each row pertains to a specific Lambert solution arrival time t_A.

To better understand the utility of PCCs, let's construct an analogy between them and contour maps. In this concept, t_D corresponds to longitude, t_A corresponds to latitude, and s_D or s_A corresponds to altitude. Indeed, interplanetary mission planners often plot contours from the digital data in PCCs we'll be discussing. Typically, these contours are roughly triangular and reminiscent of a pork chop in shape. In the case of s_D or s_A contours, we're seeking out the "valleys" and other "low spots" for our mission trajectories. Instead of contours, we'll retain digital values in a matrix and color-code them to indicate low (green), intermediate (yellow), or high (red) speeds. When we pick an acceptable value from a PCC, we'll effectively be fixing departure and arrival times for our outbound or return interplanetary cruise trajectory.

By convention, PCCs we'll discuss are rectangular matrices with t_D increasing rightward and t_A increasing downward. Depending on the t_D and t_A values spanned by columns and rows in a

[2] Because we're neglecting accelerations from Earth and Mars gravity in the heliocentric interplanetary cruise ellipse, it's important to remember these planet-centered speeds only apply a couple days after departure from or a couple days before arrival at the planet of interest.

particular PCC, some matrix elements may correspond to $\Delta t \leq 0$ (a trajectory arriving before or as it departs). Since these elements are nonsensical to our purposes, we'll see them as blanks without any values in the PCC. These void regions in an otherwise rectangular PCC matrix are typically bordered by elements corresponding to very short, but positive, Δt. Since high speed is required to cover interplanetary distances in a short time, elements bordering matrix voids are usually color-coded red.

5. Outbound Earth-To-Mars Cruise

Accurately foretelling the pace of technology is doomed to failure, but let's assume we're not ready to begin human exploration of Mars until the year 2030. Figure 2 contains heliocentric plots of Earth and Mars ephemerides projected onto the ecliptic plane during that year. Because Earth's orbit coincides with the ecliptic and Mars's orbit is inclined to the ecliptic by only 1.85°, these projections introduce negligible geometric distortion. Each planet's Figure 2 orbit is annotated with "+" time ticks every 30 days. Ticks are each labeled with the corresponding calendar date in "yyyy-mm-dd" format.

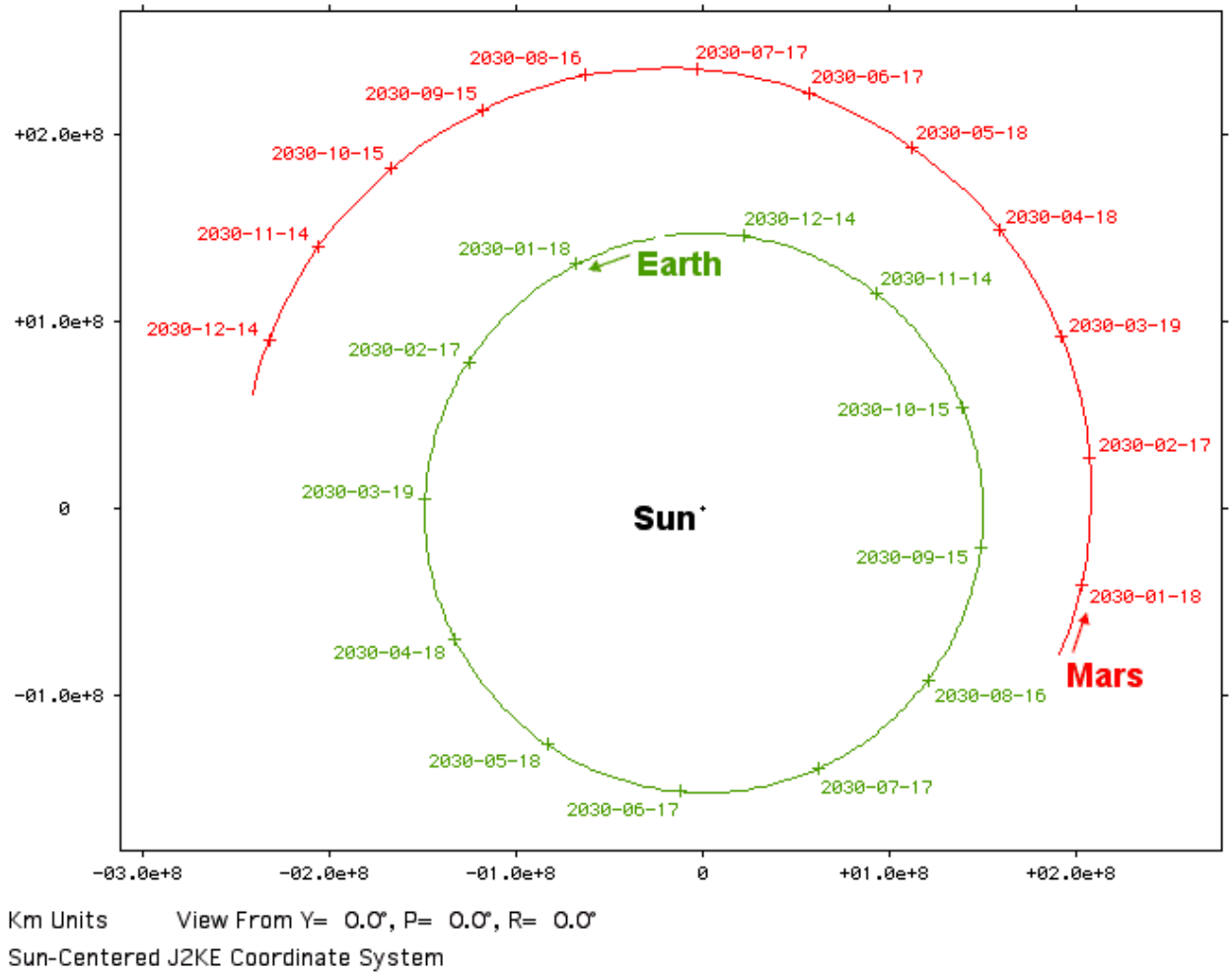

Figure 2. Earth and Mars heliocentric motion plotted during the year 2030.

Interplanetary Cruising

Casual inspection of Figure 2 shows Earth and Mars to be on different sides of the Sun throughout 2030. A closer look indicates the two planets are opposite the Sun (in conjunction) shortly after May 18, 2030. From Figure 2, we can see Earth completes an orbit about the Sun in little more than half the time Mars requires, and it's logical to assume a spacecraft cruising between the two planets would move at an intermediate heliocentric speed. We therefore need to look for Earth departure times when Mars is about to be "lapped" by Earth. By the end of 2030, Figure 2 indicates this desirable phasing relationship between Earth and Mars will occur in 2031.

Figures 3 and 4 are short-way PCCs respectively containing s_D values departing from Earth[3] and s_A values arriving at Mars in the year 2031. With 14 departure time columns and 14 arrival time rows, speeds from nearly 200 Lambert solutions appear in each PCC. Feel free to zoom in for a closer look at the numbers! Note that dates appear in these PCCs using "mm/dd/yy" format.

Mars Arrive Date	Earth Depart Date													
	1/1/31	1/11/31	1/21/31	1/31/31	2/10/31	2/20/31	3/2/31	3/12/31	3/22/31	4/1/31	4/11/31	4/21/31	5/1/31	5/11/31
5/1/31	10.338	10.494	10.691	11.065	11.732	12.826	14.701	17.714	22.584	30.992	48.419	97.198		
5/11/31	8.808	8.821	8.849	9.011	9.393	10.088	11.368	13.423	16.618	21.679	30.085	47.248	95.192	
5/21/31	7.539	7.453	7.370	7.402	7.621	8.097	9.059	10.614	12.972	16.511	21.803	30.462	47.790	96.433
5/31/31	6.486	6.333	6.180	6.139	6.274	6.644	7.452	8.748	10.664	13.420	17.254	22.894	31.972	49.498
6/10/31	5.619	5.420	5.226	5.153	5.260	5.598	6.348	7.516	9.187	11.497	14.541	18.717	24.740	34.302
6/20/31	4.919	4.686	4.473	4.398	4.514	4.867	5.611	6.716	8.240	10.270	12.833	16.182	20.677	27.055
6/30/31	4.381	4.114	3.894	3.838	3.986	4.378	5.138	6.207	7.630	9.465	11.706	14.531	18.139	22.896
7/10/31	4.033	3.700	3.472	3.443	3.633	4.069	4.846	5.886	7.230	8.917	10.923	13.388	16.425	20.230
7/20/31	3.993	3.458	3.196	3.187	3.413	3.885	4.670	5.681	6.955	8.522	10.347	12.547	15.187	18.375
7/30/31	4.716	3.455	3.070	3.049	3.293	3.783	4.563	5.540	6.750	8.215	9.894	11.890	14.238	16.996
8/9/31	8.811	3.894	3.122	3.017	3.245	3.731	4.493	5.431	6.580	7.956	9.514	11.345	13.469	15.912
8/19/31	55.522	5.543	3.450	3.100	3.255	3.710	4.440	5.335	6.425	7.721	9.175	10.869	12.814	15.016
8/29/31	62.546	14.002	4.371	3.345	3.325	3.710	4.393	5.239	6.271	7.495	8.857	10.436	12.234	14.245
9/8/31	62.689	60.559	7.249	3.909	3.484	3.735	4.348	5.139	6.112	7.268	8.548	10.027	11.701	13.556

Figure 3. Earth-centered Earth departure speed s_D (km/s) PCC.

Mars Arrive Date	Earth Depart Date													
	1/1/31	1/11/31	1/21/31	1/31/31	2/10/31	2/20/31	3/2/31	3/12/31	3/22/31	4/1/31	4/11/31	4/21/31	5/1/31	5/11/31
5/1/31	17.373	18.399	19.489	20.669	22.000	23.576	25.574	28.335	32.544	39.834	55.921	102.838		
5/11/31	15.284	16.097	16.940	17.825	18.785	19.873	21.186	22.904	25.356	29.230	36.136	51.649	97.507	
5/21/31	13.476	14.125	14.781	15.450	16.152	16.917	17.802	18.913	20.433	22.712	26.462	33.331	48.858	95.501
5/31/31	11.901	12.419	12.931	13.439	13.955	14.497	15.101	15.837	16.817	18.251	20.521	24.386	31.596	47.347
6/10/31	10.520	10.933	11.332	11.716	12.095	12.478	12.892	13.386	14.036	14.982	16.466	18.908	23.142	31.016
6/20/31	9.310	9.633	9.941	10.229	10.504	10.773	11.055	11.387	11.828	12.480	13.511	15.192	17.995	22.796
6/30/31	8.255	8.496	8.728	8.940	9.136	9.321	9.510	9.734	10.040	10.510	11.270	12.511	14.535	17.831
7/10/31	7.358	7.509	7.672	7.821	7.956	8.079	8.203	8.355	8.576	8.934	9.531	10.509	12.076	14.534
7/20/31	6.667	6.673	6.762	6.856	6.941	7.019	7.099	7.206	7.376	7.669	8.170	8.989	10.277	12.229
7/30/31	6.421	6.015	5.997	6.033	6.076	6.120	6.171	6.253	6.398	6.660	7.109	7.835	8.946	10.575
8/9/31	8.382	5.652	5.397	5.353	5.355	5.372	5.406	5.478	5.617	5.871	6.299	6.971	7.969	9.382
8/19/31	42.599	6.101	5.029	4.831	4.776	4.768	4.793	4.866	5.012	5.273	5.699	6.343	7.264	8.524
8/29/31	48.018	11.649	5.116	4.508	4.352	4.310	4.328	4.408	4.570	4.848	5.280	5.908	6.774	7.920
9/8/31	48.371	46.879	6.690	4.496	4.106	4.002	4.007	4.095	4.274	4.570	5.011	5.626	6.447	7.504

Figure 4. Mars-centered Mars arrival speed s_A (km/s) PCC.

Even a quick glance at color-coding in Figures 3 and 4 shows the desirable green regions don't completely overlap. Depending on the propulsion available to our spacecraft at departure and arrival, it may be desirable to minimize one set of speeds at the expense of the other, or strike a compromise between the two. If Earth launch postponements are likely, it may be wise to select the earliest practical departure time.

Values outlined by black boxes in Figures 3 and 4, corresponding to Earth departure on February 20 and Mars arrival on August 19 in 2031, lead to the example heliocentric cruise trajectory from Earth to Mars plotted in Figure 5. This 6-month example voyage is but one of many possible

[3] Launch vehicle manufacturers often quantify performance in terms of delivered payload mass versus achieved C_3, where $C_3 = s_D^2$. When $C_3 < 0$, escape into interplanetary space cannot be achieved for the specified payload mass.

outbound cruise trajectories. Because the outbound cruise example is inclined to the ecliptic by only 1.89°, Figure 5 plots are all projected onto the ecliptic, as were those in Figure 2.

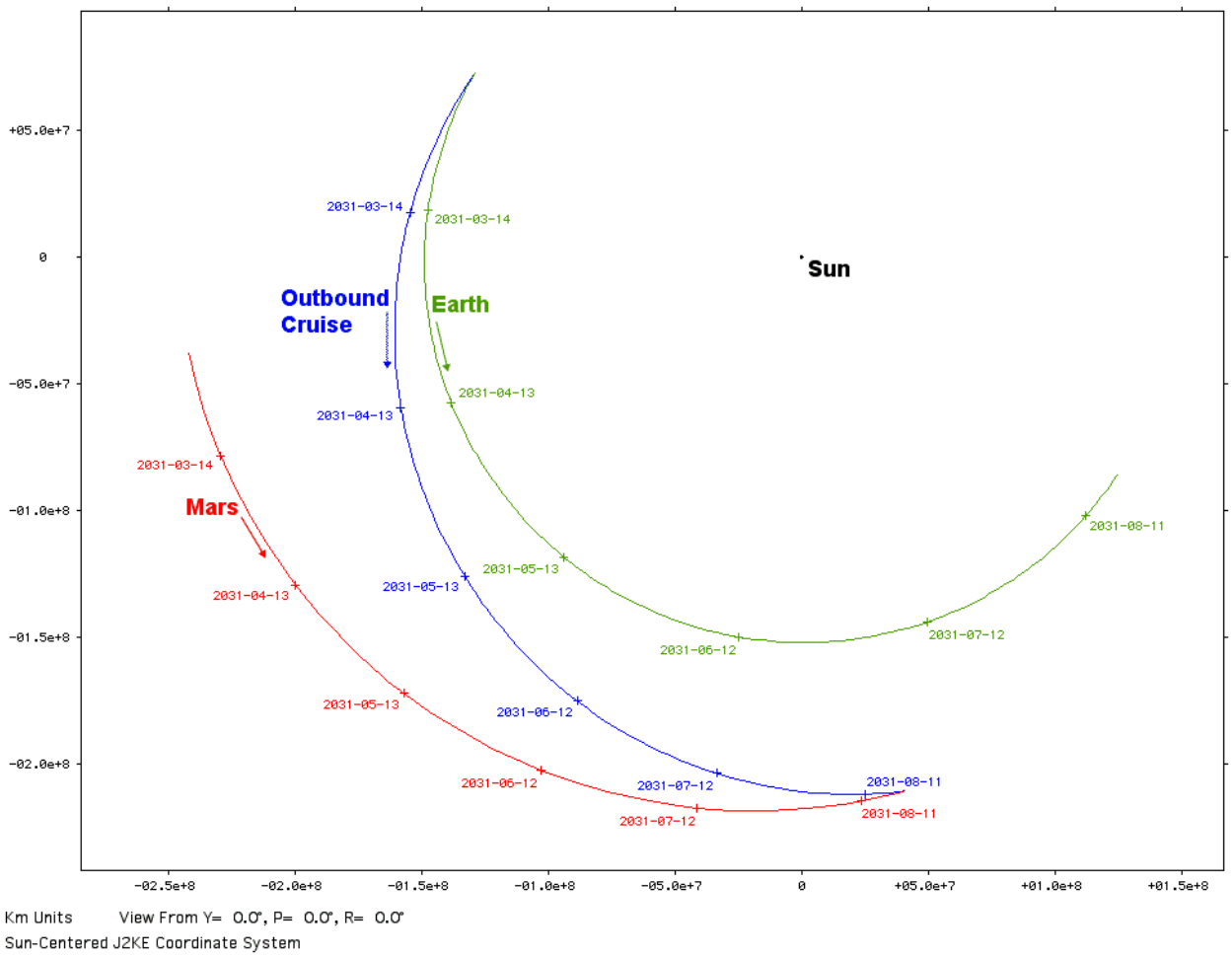

Figure 5. Heliocentric cruise trajectory departing from Earth on February 20, 2031 and arriving at Mars on August 19, 2031.

A small sub-matrix of relatively large speeds reside in the lower left corners of Figures 3 and 4. These PCC elements correspond to near-Hohmann cruises through heliocentric angles slightly less than 180°. Let's consider the 8-month cruise departing from Earth on January 1 and arriving at Mars on September 1 in 2031. This example is plotted in Figure 6. Like Figures 2 and 5, Figure 6 is heliocentric, but its perspective is different. Figures 2 and 5 are viewed from a perspective looking perpendicular to the ecliptic plane because all plots in these illustrations lie within 2° of this plane. Figure 6 is viewed from a perspective 60° away from perpendicular to the ecliptic so we can see the near-Hohmann trajectory's motion out of the ecliptic plane. Distance from the ecliptic plane in Figure 6 appears as dotted lines projected from each time tick. Earth's heliocentric orbit plane coincides with the ecliptic by definition, so no dotted lines are visible in its Figure 6 plot. Short dotted lines are associated with the Mars plot since its ecliptic inclination is 1.85°. In contrast, the near-Hohmann trajectory plot is inclined to the ecliptic by 10.41°, making for relatively prominent dotted projection lines in Figure 6. It's this motion out of the ecliptic plane that contributes relatively large speeds with respect to Earth and Mars in the

near-Hohmann regions of Figures 3 and 4. These are obviously PCC regions to avoid in our outbound mission planning!

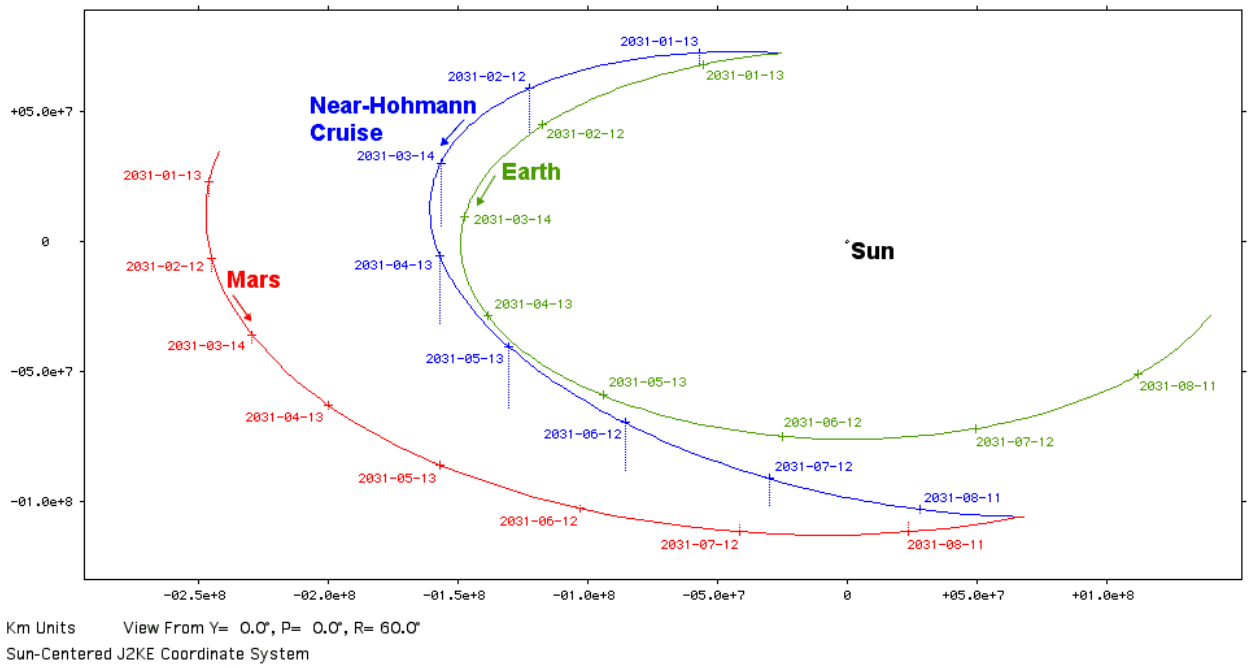

Figure 6. A nearly Hohmann heliocentric cruise trajectory departs from Earth on January 1, 2031 and arrives at Mars on September 1, 2031. Note how a straight line from departure to arrival nearly intercepts the Sun, indicating the heliocentric transfer angle θ is nearly 180°. Because Mars doesn't lie in the ecliptic plane at arrival, the cruise trajectory is forced to depart the ecliptic to a significantly large degree, as indicated by dotted blue projection lines.

6. Return Mars-To-Earth Cruise

Since we're confined to cruise intervals between Earth and Mars lasting 6 months or more, Figure 5 tells us a sobering story about our return trip. By the time we reach Mars in late 2031, Earth has already phased ahead of us in orbit around the Sun to the point a cruise lasting 6 months or so can't catch up without taking a "short-cut" inside Earth's orbit. Considering this "best departure before arrival" paradox at Mars, it's no surprise both s_D from Mars and s_A at Earth for these short-cut return trajectories would be color-coded red on a PCC.

Under interplanetary cruise constraints we've previously adopted, our only remedy is to wait at Mars until Earth begins to close in from behind again. The "cycle-time" (synodic period) required for Earth to phase completely around the Sun with respect to the Mars-Sun line is 780 days, or a bit less than 26 months. That means our return cruise short-way PCCs, as shown in Figures 7 and 8, need to span dates in the year 2033.

Interplanetary Cruising

Earth Arrive Date	Mars Depart Date 1/1/33	1/11/33	1/21/33	1/31/33	2/10/33	2/20/33	3/2/33	3/12/33	3/22/33	4/1/33	4/11/33	4/21/33	5/1/33	5/11/33
7/1/33	4.249	4.300	4.373	4.478	4.627	4.833	5.118	5.505	6.029	6.733	7.678	8.954	10.701	13.170
7/11/33	3.648	3.670	3.713	3.784	3.894	4.055	4.284	4.602	5.033	5.610	6.375	7.386	8.728	10.542
7/21/33	3.184	3.186	3.209	3.260	3.348	3.485	3.685	3.966	4.347	4.854	5.515	6.372	7.480	8.927
7/31/33	2.846	2.834	2.843	2.883	2.960	3.086	3.274	3.538	3.894	4.361	4.960	5.723	6.687	7.913
8/10/33	2.625	2.599	2.598	2.629	2.700	2.822	3.004	3.260	3.601	4.044	4.603	5.302	6.170	7.249
8/20/33	2.516	2.469	2.453	2.474	2.539	2.655	2.833	3.082	3.411	3.834	4.362	5.013	5.810	6.785
8/30/33	2.534	2.444	2.400	2.401	2.452	2.558	2.726	2.964	3.281	3.684	4.183	4.795	5.534	6.428
9/9/33	2.762	2.557	2.446	2.404	2.425	2.509	2.659	2.880	3.178	3.559	4.031	4.605	5.295	6.122
9/19/33	3.721	2.996	2.662	2.507	2.462	2.502	2.620	2.815	3.088	3.443	3.886	4.424	5.069	5.837
9/29/33	24.409	5.749	3.545	2.872	2.620	2.557	2.613	2.765	3.004	3.328	3.738	4.239	4.842	5.557
10/9/33	42.419	42.426	34.596	5.514	3.304	2.785	2.673	2.742	2.928	3.211	3.583	4.047	4.607	5.272
10/19/33	42.377	42.587	42.788	42.940	41.017	4.882	3.046	2.798	2.874	3.097	3.426	3.849	4.366	4.983
10/29/33	42.205	42.461	42.718	42.976	43.230	43.470	43.297	3.828	2.914	2.998	3.268	3.647	4.121	4.692
11/8/33	41.945	42.242	42.541	42.842	43.143	43.445	43.744	44.041	44.308	2.951	3.106	3.445	3.878	4.402

Figure 7. Mars-centered Mars departure speed s_D (km/s) PCC.

Earth Arrive Date	Mars Depart Date 1/1/33	1/11/33	1/21/33	1/31/33	2/10/33	2/20/33	3/2/33	3/12/33	3/22/33	4/1/33	4/11/33	4/21/33	5/1/33	5/11/33
7/1/33	11.175	11.436	11.708	11.994	12.298	12.627	12.989	13.396	13.869	14.436	15.146	16.074	17.351	19.220
7/11/33	9.536	9.742	9.954	10.174	10.405	10.650	10.915	11.209	11.543	11.937	12.420	13.040	13.873	15.054
7/21/33	8.086	8.245	8.408	8.576	8.749	8.931	9.124	9.335	9.572	9.847	10.181	10.605	11.170	11.960
7/31/33	6.790	6.908	7.029	7.153	7.280	7.412	7.552	7.702	7.870	8.064	8.300	8.600	9.001	9.561
8/10/33	5.727	5.806	5.889	5.975	6.065	6.159	6.258	6.365	6.486	6.627	6.800	7.025	7.329	7.756
8/20/33	4.866	4.900	4.944	4.997	5.055	5.118	5.188	5.266	5.356	5.465	5.603	5.786	6.038	6.393
8/30/33	4.275	4.238	4.232	4.244	4.271	4.308	4.355	4.414	4.487	4.581	4.705	4.872	5.104	5.429
9/9/33	4.156	3.956	3.856	3.809	3.795	3.804	3.832	3.877	3.942	4.032	4.154	4.322	4.551	4.867
9/19/33	5.175	4.240	3.846	3.661	3.575	3.543	3.546	3.578	3.638	3.727	3.852	4.024	4.257	4.568
9/29/33	35.542	7.941	4.880	4.029	3.712	3.584	3.543	3.554	3.603	3.690	3.816	3.989	4.220	4.524
10/9/33	62.832	62.569	50.393	7.548	4.596	3.967	3.785	3.745	3.773	3.849	3.968	4.134	4.355	4.643
10/19/33	62.932	62.997	63.016	62.916	59.557	6.652	4.368	4.061	4.030	4.084	4.190	4.343	4.548	4.814
10/29/33	62.797	62.929	63.033	63.107	63.145	63.126	62.390	5.398	4.432	4.424	4.513	4.649	4.833	5.072
11/8/33	62.510	62.700	62.862	62.997	63.105	63.183	63.232	63.247	63.174	4.791	4.872	4.993	5.148	5.352

Figure 8. Earth-centered Earth arrival speed s_A (km/s) PCC.

Slightly favoring minimal Mars departure speed over that at Earth arrival, PCC elements outlined by black boxes in Figures 7 and 8 indicate a return cruise departing from Mars January 21 and arriving at Earth on August 30 in 2033 has been selected as an example for plotting in Figure 9. We might select a similar return option if our spacecraft will use acceleration from Earth atmospheric friction to slow its return speed. Should Earth return require propulsive braking, however, a delayed Mars departure and delayed Earth return may be advisable. Because the return cruise has ecliptic inclination of only 1.66°, Figure 9 perspective is again normal to the ecliptic as in Figures 2 and 5.

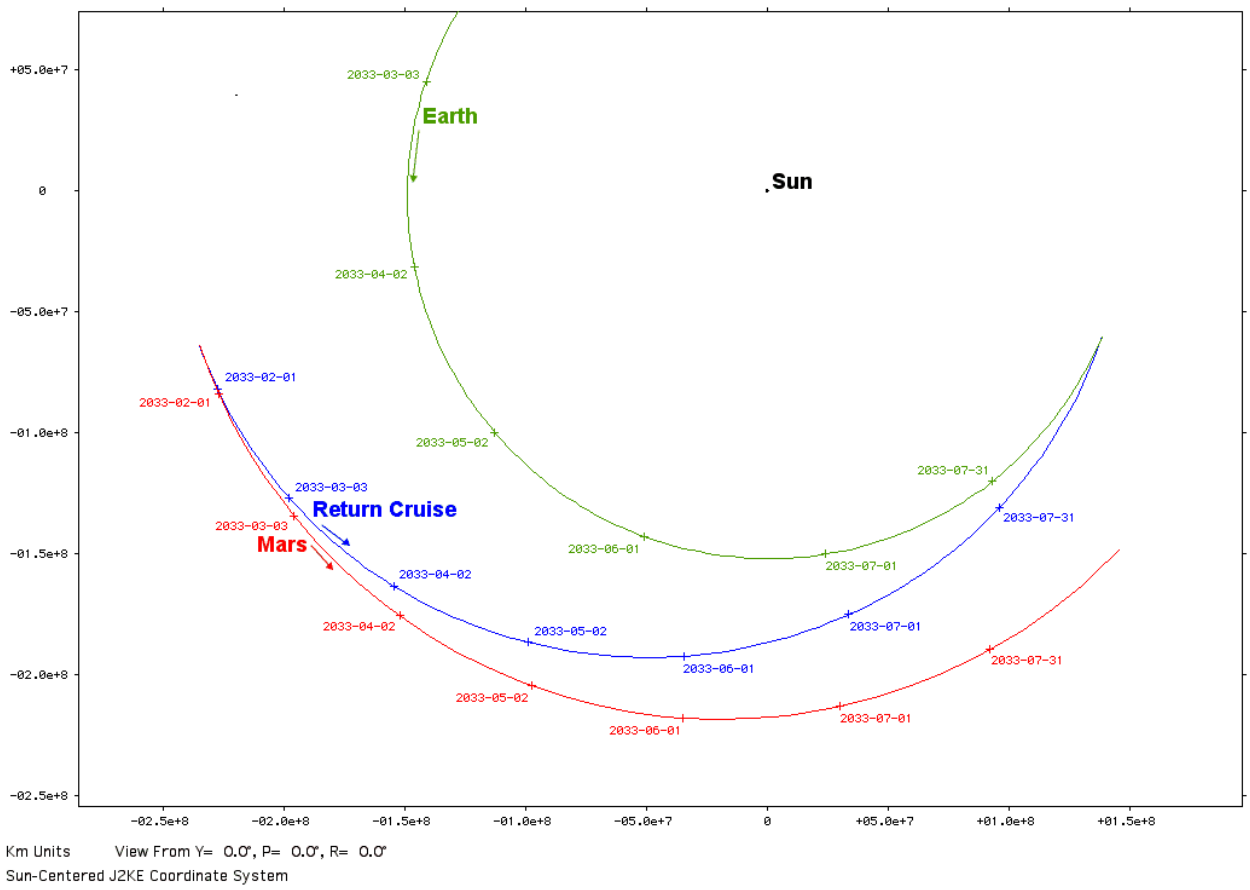

Figure 9. Heliocentric cruise trajectory departing from Mars on January 21, 2033 and arriving at Earth on August 30, 2033.

7. Planet-Centered Trajectory Transfers To And From Interplanetary Space

In departing from (or arriving at) a planet, we generally want to start from (or end in) a circular orbit with planet-centered radius r_C and moving at planet-centered speed v_C. To transfer between a planet-centered departure or arrival hyperbola and the circular orbit, a change-in-velocity magnitude Δv is necessary. For simplicity, we'll assume this Δv is provided instantaneously by propulsion, but it will require at least 5 to 10 minutes to achieve Δv depending on propulsive thrust and spacecraft mass. In the arrival case, it may also be possible to obtain Δv and initiate transfer to the desired circular orbit using friction from passage through the planet's upper atmosphere in a process called aero-capture.

When we obtain an s_D (or s_A) value from a PCC, we can't immediately relate that speed to the required transfer Δv from (or to) the circular orbit. That's because these asymptotic speeds are only valid at the edge of interplanetary space, days away from actual planetary departure or arrival. This "gravitational frontier" is the appropriate region in which to connect a departure or arrival planet-centered hyperbolic trajectory with the heliocentric interplanetary cruise ellipse in accord with patched conic theory. On the "flat" periphery of a planet's 3-dimensional gravity

well, less than one million km across in the case of Earth or Mars, the hyperbola and ellipse blend into each other and are effectively indistinguishable. To compute Δv, we must first understand how our spacecraft's planet-centered energy varies in the planet's gravity well.

Early in the twentieth century, Hermann Oberth discovered that change in specific kinetic energy[4] exerted by a specified Δv depends on the speed at which Δv is applied[5]. This principle has come to be known as the *Oberth effect*. If our spacecraft has planet-centered velocity $\boldsymbol{v}$ initially, the change in specific kinetic energy ΔE resulting from a change-in-velocity $\Delta \boldsymbol{v}$ can be expressed as follows.

$$\Delta E = \frac{\left(\boldsymbol{v} + \Delta \boldsymbol{v}\right) \bullet \left(\boldsymbol{v} + \Delta \boldsymbol{v}\right) - \boldsymbol{v} \bullet \boldsymbol{v}}{2}$$

$$\Delta E = \frac{2\, \boldsymbol{v} \bullet \Delta \boldsymbol{v} + \Delta v^2}{2} \tag{7.1}$$

For a fixed Δv, Equation 7.1 has two ΔE extrema related to *steering*, the direction in which $\Delta \boldsymbol{v}$ is applied. A maximum ΔE will result if $\Delta \boldsymbol{v}$ is applied in the same direction as $\boldsymbol{v}$, and a minimum ΔE will result if $\Delta \boldsymbol{v}$ is applied in the direction opposed to $\boldsymbol{v}$. In either case, the extremum will be enhanced in direct proportion to v.

How can we maximize v and the Oberth effect as we arrive at (or depart from) a planet? An intuitive answer is suggested by visualizing our spacecraft's fall into a planet's gravity well along a hyperbolic approach trajectory. If we start at s_A and fall as far as possible into this well, minimizing r_C without venturing too deep in the planet's atmosphere, potential energy will be transformed into kinetic energy to the greatest extent possible, thereby maximizing v. We can quantify this effect with the *vis viva* energy integral given in Equation 7.2.

$\mu \equiv$ reduced mass of the planet, equal to the product of the universal gravitation constant with the sum of the planet's mass and our spacecraft's relatively miniscule mass
$r \equiv$ planet-centered spacecraft distance
$a \equiv$ planet-centered conic trajectory semi-major axis

$$v = \sqrt{\mu \left(\frac{2}{r} - \frac{1}{a} \right)} \tag{7.2}$$

Depending on the conic trajectory of interest, Equation 7.2 can take on multiple specific forms. In the case of a circular trajectory, $a = r$, and Equation 7.3 results.

[4] With *specific* kinetic energy, we ignore our spacecraft's mass and are only concerned with changes in its speed. We'll study propellant mass computations required to obtain Δv later.
[5] Reference NASA TT F-622, "Ways To Spaceflight", a translation of Oberth's "Wege zur Raumschiffahrt" published by R. Oldenbourg Verlag in Munich-Berlin during 1929, p. 200. This document may be downloaded from http://ntrs.nasa.gov/archive/nasa/casi.ntrs.nasa.gov/19720008133_1972008133.pdf [accessed 9 October 2011].

$$v_C = \sqrt{\frac{\mu}{r}} \tag{7.3}$$

In the case of an arrival or departure hyperbola, consider Equation 7.2 under asymptotic conditions with $r = \infty$. Planet-centered motion at infinite distance is hyperbolic excess speed v_{HE}. Thus, Equation 7.2 leads to the following expression valid for any specific hyperbola.

$$-\frac{1}{a} = \frac{v_{HE}^2}{\mu} \tag{7.4}$$

When Equation 7.4 is substituted into Equation 7.2, a very useful hyperbolic trajectory energy equation results.

$$v = \sqrt{\frac{2\mu}{r} + v_{HE}^2} \tag{7.5}$$

The significance of Equation 7.5 is v_{HE}'s equivalence to an s_D or s_A value obtained from a PCC. With a PCC value substituted into Equation 7.5 along with $r = r_C$, hyperbolic departure or arrival speed can be computed for the desired circular orbit radius. Equations 7.3 and 7.5 confirm our earlier intuitive assertion that the Oberth effect and v are maximum when r, and therefore r_C, are minimal.

In summary, Δv is simply Equation 7.3 subtracted from Equation 7.5 when both are evaluated with $r = r_C$. At planetary departure, we want the greatest possible ΔE, so Equation 7.1 has our spacecraft flying "nose forward" to align $\boldsymbol{\Delta v}$ with $\boldsymbol{v}$. Conversely, Equation 7.1 has us flying "tail forward" at planetary arrival. Precision avionics systems in our spacecraft will break $\boldsymbol{\Delta v}$ into tiny segments and ensure steering relationships with respect to $\boldsymbol{v}$ are satisfied every few seconds.

Table 1 provides data relevant to evaluating the energy integral near Earth, Mars, and the Moon. The value of R provides the radius of each body's approximate spherical surface, and H_0 is the minimum recommended height above R for safe orbit motion. To maximize the Oberth effect, we'll therefore use $r_C = R + H_0$ in a particular planet-centered context.

Table 1. A collection of useful constants for evaluating the energy integral associated with conic trajectories centered on Earth, Mars, and the Moon.

	μ (km^3/s^2)	R (km)	H_0 (km)
Earth	398,600.440	6378.136	185
Mars	42,828.3	3394.0	380
Moon	4902.798	1737.53	100

Let's perform a numeric example of energy integral computations using a Mars arrival context. Procedural steps and results follow.

1) Obtain $\mu = 42{,}828.3$ km^3/s^2 for Mars-centered trajectories from Table 1.

2) Compute $r_C = 3394.0 + 380 = 3774.0$ km for Mars values in Table 1.

3) Obtain $v_{HE} = 4.768$ km/s from the boxed value in Figure 4.

4) Substitute Step 2's r_C value for r in Equation 7.5 and obtain $v = 6.740$ km/s. This is the speed with which our spacecraft arrives at r_C, and its motion is assumed tangent to the desired circular orbit to minimize steering inefficiencies in accord with Equation 7.1. Because any trajectory tangent to a circular orbit has zero planet-centered radial velocity, r_C is also the arrival hyperbola's *periapsis* or closest approach to Mars.

5) Substitute Step 2's r_C value for r in Equation 7.3 and obtain $v_C = 3.369$ km/s.

6) Assuming the speeds obtained in Steps 4 and 5 correspond to Mars-centered velocity vectors with identical directions, obtain $\Delta v = v - v_C = 3.371$ km/s. This is the degree to which Mars-centered speed must be reduced by a Mars orbit insertion (MOI) maneuver in accord with the Figure 5 heliocentric trajectory.

Similar procedures can be used to compute Δv in Earth departure, Mars departure, and Earth return contexts. Small bodies, such as near-Earth objects (NEOs), effectively have $\mu = 0$. In such cases, there is no gravity well to fall into from interplanetary space, and Equation 7.5 reduces to $v = v_{HE}$. If Earth return is planned to utilize atmospheric braking, $r_{EI} = 6378.136 + 121.92 = 6500.056$ km can be used to determine Earth-centered *entry interface* speed v_{EI} when r_{EI} is substituted for r in Equation 7.5. At r_{EI}, thermal and mechanical loads on a returning spacecraft first become appreciable and will rapidly increase with further descent. A typical Earth return from the Moon has $v_{EI} = 11$ km/s. With a crewed entry vehicle's mass near 10,000 kg, safe Earth entry and landing will challenge foreseeable technology at $v_{EI} > 12$ km/s.

8. The Rocket Equation's Tyranny

The rocket equation may take many forms. One of them appears in Equation 8.3 below, where "exp" denotes the natural exponential function whose base is approximately 2.71828.

$m_A \equiv$ spacecraft total mass after Δv is imparted
$m_Y \equiv$ payload mass aboard spacecraft while Δv is imparted
$m_P \equiv$ spacecraft propellant mass required to impart Δv
$m_B \equiv$ spacecraft total mass before Δv is imparted $= m_A + m_Y + m_P$ (8.1)
$g \equiv$ Earth gravity acceleration $= 0.00980665$ km/s^2
$I_{SP} \equiv$ propulsion system specific impulse used to impart Δv
$v_X \equiv$ propulsion system exhaust speed $= g\, I_{SP}$ (8.2)
$m_B = (m_A + m_Y) \exp(\Delta v / v_X)$ (8.3)

From Equation 8.3, it's evident we prefer propulsion systems with the highest practical I_{SP} and v_X performance values. Each time Δv increases by v_X, the ratio $m_B / (m_A + m_Y)$ increases by a factor of 2.72 just from increased m_P. If our spacecraft's propellant tanks aren't designed to

accommodate increased m_P, m_A must also be increased. This snowballing effect on m_B can be compounded when a mission requires multiple Δv propulsive impulses. We'll call each such impulse a *stage*. During a mission to Mars, stages might include Earth departure, Mars arrival, Mars descent, Mars ascent, Mars departure, and Earth return. Each stage has its own Δv contribution to make, and such is the tyranny of the rocket equation.

The I_{SP} associated with a propulsion system is defined as the time this system consumes a unit of propellant in Earth weight (the product of propellant mass and g) while generating a unit of propulsive thrust. Examples of propulsion systems and the efficiency they achieve as measured by I_{SP} appear in Table 2.

Table 2. Different propulsion systems are listed for comparison. Note the general trend in which thrust reduces with increased efficiency (I_{SP}). A range of I_{SP} values is given for systems operating at sea level and in a near vacuum.

System	Propellant	Thrust (N)	I_{SP} (s)
Shuttle SRB	Storable solids	12 million	242 to 268
Saturn V F-1	LOX and storable RP-1	6.77 million	263
Shuttle OMS	Storable hypergolics	27,000	313
Aerojet Prototype	LOX and LCH_4	24,000	345
Saturn V J-2	LOX and LH_2	1.033 million	421
SSME (RS-25)	LOX and LH_2	1.8 million	363 to 453
Nuclear Thermal (NERVA)	LH_2	333,600	850
Solar Electric (*Dawn*)	Storable Xe	0.090	3100
VASIMR VX-200	Storable Ar	5	5000

The type of propulsion system to be used in a particular stage depends on multiple factors. Cryogenic propellant such as liquid oxygen (LOX), liquid hydrogen (LH_2) or liquid methane (LCH_4) may be impractical to store aboard our spacecraft for long periods. Radioactive systems will be inappropriate for use near Earth or other sensitive habitats. Highly efficient systems with low thrust cannot be used during launch from a planetary surface if weight greatly exceeds thrust. Likewise, low-thrust systems may be inappropriate for human transport because they tend to slowly spiral out of or into a planet's gravity well, adding significantly to departure or arrival time. Figure 10 is an example of such a trajectory spiral. It illustrates a 19-day segment of the robotic *Dawn* probe's arrival at main belt asteroid (4) Vesta, whose very shallow gravity well has $\mu = 17.8\ km^3/s^2$.

Interplanetary Cruising

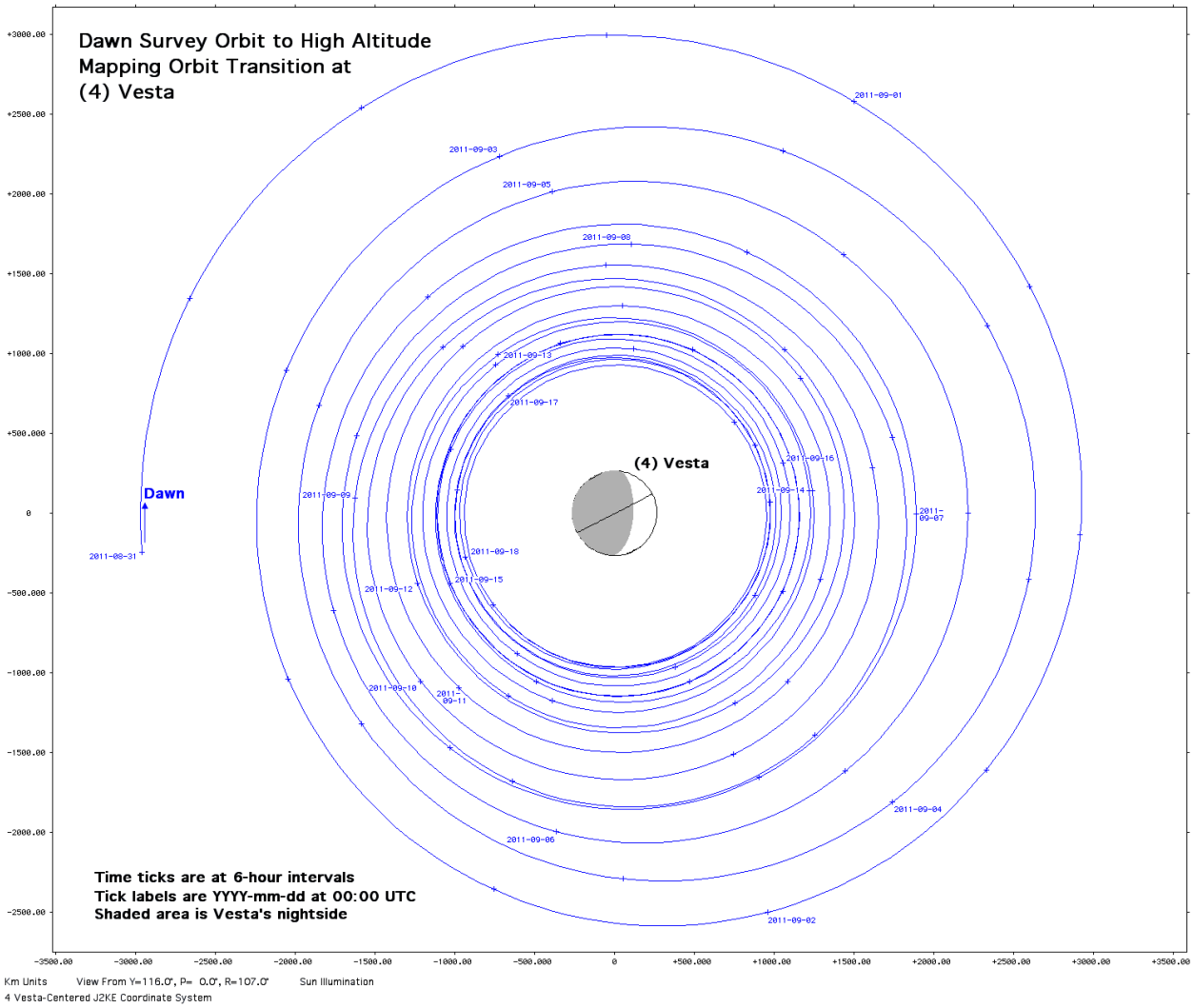

Figure 10. The robotic spacecraft *Dawn*'s descent at main belt asteroid (4) Vesta is plotted from survey orbit departure to high altitude mapping orbit arrival 19 days later under solar electric propulsion (SEP). Acceleration from SEP exerted on *Dawn* is about 0.1 mm/s^2, but this acceleration can be maintained for 2000 days with the 425 kg of Xe loaded at launch.

Typically, m_B on a given stage (or perhaps its associated m_P) is a component of m_Y on the previous stage. Because earlier stages tend to be dependent on later ones, it's usually necessary to obtain masses for a later stage first and work chronologically backward though a mission's timeline. Exceptions can arise, however. It's possible to pre-emplace components for certain stages such that our spacecraft doesn't have to transport this mass from Earth. We could send a Mars habitat from Earth to Mars before our spacecraft even leaves Earth, but that only turns one Earth departure into two. It doesn't reduce total mass departing Earth for our mission, but a technique called *in-situ resource utilization* (ISRU) could make dramatic reductions. For example, if m_P can be produced from material on Mars local to our planned landing site, only the material processing mass has to be pre-emplaced. We'd then have easy access to the equivalent of an interplanetary service station on Mars at which to "tank up" before starting our return journey. The ISRU concept will likely become a means to establish new extraterrestrial

economies some day. As with any successful business, the key to profitable ISRU is the old adage "location, location, location". The rocket equation's tyranny prohibits taking advantage of pre-emplaced mass if a detour requiring appreciable Δv is necessary to access that mass.

The $m_A + m_Y$ factor in Equation 8.3 can be augmented with additional terms as our spacecraft's design requires. For example, we can redefine m_A as $m_{A'}$, with the latter excluding propulsion system mass m_S (tankage, propellant lines, and engines). Then we can express m_S according to Equation 8.4 such that it scales linearly with m_P.

$k \equiv$ dimensionless constant near 0.15 for chemical propulsion systems in which combustion between a fuel and an oxidizer provides thrust

$$m_S = k\, m_P \tag{8.4}$$

In terms of $m_{A'}$ and m_S, the rocket equation is expressed as Equation 8.5.

$$m_P + k\, m_P + m_{A'} + m_Y = (k\, m_P + m_{A'} + m_Y) \exp(\Delta v / v_X) \tag{8.5}$$

Equation 8.6 is a useful solution for m_P obtained from Equation 8.5 in terms of other mass components, k, Δv, and v_X. All these quantities should be known from our spacecraft and mission design at a particular stage.

$$m_P = \frac{\left(m_{A'} + m_Y\right)\left(\exp\left[\Delta v / v_X\right] - 1\right)}{1 + k\left(1 - \exp\left[\Delta v / v_X\right]\right)} \tag{8.6}$$

Yet another aspect of the rocket equation's tyranny is imbedded in Equation 8.6's denominator. As Δv increases from zero toward a critical value Δv_K, m_P increases toward $+\infty$. At $\Delta v > \Delta v_K$, nonsensical negative m_P is obtained from Equation 8.6. Consequently, even if special relativity is ignored, a propulsive system cannot deliver unlimited Δv. Equation 8.7 is the formula for Δv_K obtained by setting the denominator of Equation 8.6 to zero and solving for Δv. The natural logarithm function appears as "ℓn" in Equation 8.7.

$$\Delta v_K = v_X\, \ell n\left(1 + 1/k\right) \tag{8.7}$$

Let's apply formulae from this section to the MOI stage numeric example related previously. Procedural steps and results follow.

1) From the MOI stage example, we already have $\Delta v = 3.371$ km/s.

2) Assume we have a high-thrust nuclear thermal propulsion system supporting the MOI stage with $I_{SP} = 800$ s and $k = 0.15$. Equation 8.2 gives $v_X = 7.845$ km/s for this system. Equation 8.7 indicates this system can perform MOI because $\Delta v_K = 15.980$ km/s > Δv.

3) Assume our spacecraft's mass without propellant or propulsive systems is $m_{A'} = 180{,}000$ kg. Further assume our spacecraft carries $m_Y = 55{,}000$ kg to support operations in the

vicinity of Mars. Equation 8.6 produces m_P = 137,213 kg for the MOI stage, and Equation 8.4 determines m_S = 20,582 kg. From the left side of Equation 8.5, we can infer m_B = 392,795 kg. This is a mass not very different from that of International Space Station (ISS) when its assembly was completed in 2011. Unlike ISS, this m_B has to be sent on its way toward Mars with an Earth-centered asymptotic speed s_D = 3.710 km/s (reference the boxed value in Figure 3) as it enters interplanetary space.

In the Earth departure stage preceding the MOI stage, the m_B computed in Step 3 must be absorbed by $m_{A'}$ or m_Y. Because m_P for the Earth departure stage will be even greater than that for MOI, m_S will grow proportionally. It may be advisable to jettison some of the Earth departure m_S as otherwise dead weight if its capacity can't be used later in the mission. Drop tanks, whose propellant is consumed during Earth departure, can facilitate this jettison.

9. Conclusion

Welcome back to Earth! Our example round trip requires an outbound cruise to Mars lasting 6 months, a loiter period at Mars lasting 17 months, and a return to Earth cruise lasting 7 months. We'll be away from home a total of 30 months, or 2.5 years. Although most of our journey is presumably spent exploring Mars, using warp drive for propulsion is starting to sound better and better!

We now have a basic understanding of considerations, techniques, and terminology applicable to interplanetary spacecraft and mission design. It's like having a rocket scientist learner's permit to drive on the interplanetary superhighway. Enjoy the ride, and be careful out there!